Available online at www.sciencedirect.com
ScienceDirect
Journal of Sound and Vibration 302 (2007) 1000–1017
JOURNAL OF SOUND AND VIBRATION
www.elsevier.com/locate/jsvi

Acoustic attenuation performance of perforated dissipative mufflers with empty inlet/outlet extensions

F.D. Denia[a,*], A. Selamet[b], F.J. Fuenmayor[a], R. Kirby[c]

[a]*Departamento de Ingeniería Mecánica y de Materiales, Universidad Politécnica de Valencia, Camino de Vera s/n, 46022 Valencia, Spain*
[b]*Department of Mechanical Engineering and The Center for Automotive Research, The Ohio State University, Columbus, OH 43212, USA*
[c]*Department of Mechanical Engineering, Brunel University, Uxbridge, Middlesex UB8 3PH, England*

Received 28 September 2006; received in revised form 10 January 2007; accepted 11 January 2007
Available online 20 February 2007

Abstract

The acoustic behavior of perforated dissipative circular mufflers with empty extended inlet/outlet is investigated in detail by means of a two-dimensional (2D) axisymmetric analytical approach that matches the acoustic pressure and velocity across the geometrical discontinuities, and the finite element method (FEM). The complex characteristic impedance, wavenumber, and perforation impedance are taken into account to evaluate the axial wavenumber in the fibrous material and the central perforated pipe. Two different analytical procedures are presented that allow the computation of the modal wave coefficients for the muffler sections. Benchmarking against FE calculations exhibited an excellent agreement. Both approaches are also compared with experimental work for further validation. Several effects are examined, including the extended inlet/outlet ducts, absorbent resistivity, the porosity of the perforations, and the muffler dimensions, and compared with muffler configurations of earlier studies, such as reactive extended inlet/outlet expansion chambers, dissipative mufflers without extensions, and mufflers with absorbent-filled extensions. It is shown that the use of empty extensions leads to quarter-wave resonances providing an improved acoustic performance of the muffler at low to mid frequencies. Also, the presence of sound-absorbing material partially retains the desirable behavior of the dissipative mufflers at higher frequencies.

1. Introduction

The presence of extended inlet/outlet ducts in a reactive expansion chamber is known to provide an acoustic attenuation performance in which a combination of broadband domes and resonant peaks is found below the onset of the first excited higher-order mode [1–3]. By a suitable selection of the lengths of extended ducts, it is possible to match the resonances with the pass-band frequencies, thus improving the acoustic behavior over a wide frequency range for single-chamber mufflers [3] as well as multiple-chamber configurations [4]. This enhancement of the transmission loss is primarily associated with the low and mid frequency range, where planar propagation dominates the acoustic field.

*Corresponding author. Tel.: +34 96 387 96 20; fax: +34 96 387 76 29.
E-mail address: fradegu1@mcm.upv.es (F.D. Denia).

0022-460X/$ - see front matter © 2007 Elsevier Ltd. All rights reserved.
doi:10.1016/j.jsv.2007.01.005

Nomenclature

A_n, B_n, C_n, D_n, E_n wave coefficients in regions A, B, C, D, and E
c_0 speed of sound in air
$\tilde{c}$ complex speed of sound in the absorbing material
d_h perforate hole diameter
f frequency
H_υ υth-order Struve function
j imaginary unit
J_υ υth-order Bessel function of the first kind
k_0 wavenumber in air
$\tilde{k}$ complex wavenumber in the absorbing material
$k_{z,A,n}$, $k_{z,B,n}$, $k_{z,C,n}$, $k_{z,D,n}$, $k_{z,E,n}$ axial wavenumbers in regions A, B, C, D, and E
$k_{r,A,n}$, $k_{r,B,n}$, $k_{r,D,n}$, $k_{r,E,n}$ radial wavenumbers in regions A, B, D, and E
$k_{r,C,n}$, $\tilde{k}_{r,C,n}$ radial wavenumbers in region C, air and absorbing material
N maximum mode number for series expansion
n mode number
L_B, L_C, L_D lengths of regions B, C, and D
P_A, P_B, P_C, P_D, P_E acoustic pressure in regions A, B, C, D, and E
R flow resistivity of the absorbing material
r radial coordinate
R_1, R_2 radii of inlet/outlet ducts and chamber
s mode number of weighting functions
TL transmission loss
t_p perforated screen thickness
U_A, U_B, U_C, U_D, U_E acoustic axial velocity in regions A, B, C, D, and E
U_r acoustic radial velocity across central perforated pipe
Y_υ υth-order Bessel function of the second kind
Z_0 characteristic impedance of air
$\tilde{Z}$ complex characteristic impedance of the absorbing material
z_1, z_2 axial coordinates

Greek symbols

Γ Euler's gamma function
ρ_0 air density
$\tilde{\rho}$ complex density in the absorbing material
σ porosity of perforated screen
$\psi_{A,n}(r)$, $\psi_{B,n}(r)$, $\psi_{C,n,P}(r)$, $\psi_{D,n}(r)$, $\psi_{E,n}(r)$ pressure eigenfuntions for regions A, B, C, D, and E
$\psi_{C,n,U}(r)$ velocity eigenfuntion for region C
ω angular frequency
$\tilde{\zeta}_{p1}, \tilde{\zeta}_{p2}, \tilde{\zeta}_{p3}$ nondimensionalized acoustic impedances of perforated central pipe, left and right lateral screens

However, alternative attenuation procedures may be required for high frequencies, with the use of fibrous material being the most common approach in this case. Dissipative ducts and silencers have been modeled both numerically [5–8] and analytically [9–17]. The latter category includes both one-dimensional (1D) and multidimensional approaches, and presents an alternative to purely numerical schemes. Wang [9] presented a 1D model based on a decoupling scheme to obtain the acoustic performance of resonators with absorbing material, including the mean flow and a central perforated tube. For some geometrically simple configurations, such as circular mufflers, Peat [10] and Kirby [11] derived explicit algorithms based on approximations of Bessel and Neumann functions, while avoiding an iterative process and providing a faster computation. Kirby also considered the convective effect of the mean flow and a central perforated duct. In addition, extra terms in the approximations of the Bessel and Neumann functions are included in comparison with Ref. [10], which enabled the modeling of larger silencers and/or higher frequencies. Both studies provided comparisons with some experimental results, showing a reasonable agreement. Cummings and Chang [12] considered a circular dissipative muffler without perforated pipe and included the mean flow in the central passage and in the absorbing material. They presented an analytical approach based on the mode-matching method and obtained good agreement between predictions and measurements with six modes evaluated from the transversal eigenequation. In Ref. [13], the acoustic behavior of circular dissipative mufflers is studied in detail by a 2D analytical approach, while varying the fibrous material resistivity and thickness, and the chamber diameter. Comparison with boundary element results and experimental measurements showed good

agreement for a number of modes equal or greater than nine. Selamet et al. [14] extended this analysis to consider the presence of a concentric perforated screen and studied the effect of absorbent resistivity and thickness, screen porosity, and chamber diameter and length. A reasonable agreement was obtained between the analytical and numerical predictions and the measurements. For mufflers with arbitrary (but axially uniform) cross-section, Glav [15] derived a transfer matrix for dissipative silencers, in the absence of mean flow and perforations. The acoustic field inside the muffler was evaluated by combining the point collocation technique to solve the tranversal eigenvalue problem, and the mode-matching method in the inlet/outlet. For dissipative mufflers with mean flow and a concentric perforated pipe, Kirby [16] presented a method whereby a 2D finite-element eigenvalue calculation is combined with a point collocation matching scheme in the inlet/outlet ducts. The method is shown to provide good agreement with the experimental results, and the computational effort is reduced compared with a complete three-dimensional numerical approach. These studies have illustrated the suitability of dissipative configurations for noise control in automotive exhaust systems, since their broadband attenuation is obtained predominantly in the mid- to high-frequency range.

Few reported attempts are available on the combination of the reactive behavior of extended ducts and the dissipative effects of absorbing material. Selamet et al. [18] studied a hybrid silencer combining a Helmholtz resonator and two dissipative chambers by the boundary element method. This configuration was shown to provide an improved transmission loss at low frequencies, while keeping a reasonable level of attenuation in the high-frequency range. Recently, Selamet et al. [19] and Denia et al. [20] have studied the effect of variations in the internal structure of the dissipative silencer. These works presented 2D analytical approaches for the consideration of absorbent-filled and empty extended inlet and outlet ducts, respectively, and a good comparison with experiments and numerical results was shown for some specific configurations. The combination of reactive and dissipative effects in hybrid mufflers can be further explored in view of its potential contribution to the improvement of the acoustic performance. The objective of the present work is therefore to investigate in detail the acoustic characteristics of perforated dissipative mufflers with empty extended inlet/outlet. The extensions are purely reactive, that is, the absorbing material is only confined to the central region of the chamber, thus enabling an approximate control of the quarter-wave resonator frequencies. To achieve this objective, an analytical approach is presented, and a benchmark with FE calculations is carried out to provide validation. Both approaches are also compared with experimental work for further validation.

Following this Introduction, the 2D axisymmetric analytical approach is described, in two basic steps: (1) the evaluation of the coupled axial wavenumber for the fibrous material and central perforated pipe section; and (2) the consideration of the conditions to be satisfied by the acoustic field in the axial direction at the muffler discontinuities. These steps lead to an algebraic system of equations from which the wave coefficients in the pertinent ducts are evaluated. Different procedures for the generation of this system of equations are presented, whose suitability is analyzed by comparison with finite element method (FEM) and experiments for selected configurations. A number of geometries are then analyzed, including the effect of inlet/outlet lengths, fiber resistivity, porosity of the perforated surfaces, and muffler dimensions. In addition, comparison is also given with different muffler configurations of earlier works, such as reactive extended inlet/outlet chambers, dissipative mufflers without extensions and mufflers with absorbent-filled extensions.

2. Mathematical approach

Fig. 1 shows the geometry of a perforated dissipative circular muffler with empty inlet/outlet extensions. The total length L is divided into an extended inlet of length L_B, a central chamber of length L_C, and an extended outlet of length L_D. A homogeneous and isotropic sound-absorbing material characterized by the complex density $\tilde{\rho}$ and speed of sound $\tilde{c}$ is placed in the central region of the chamber between radii R_1 and R_2, and confined by perforated screens whose nondimensionalized acoustic impedances are $\tilde{\zeta}_{pi}$, with $i = 1, 2, 3$. The air in the central inner duct as well as in the extended annular regions is characterized by the speed of sound c_0 and density ρ_0. Five regions denoted by A, B, C (including both the central inner duct and the sound-absorbing material), D, and E are depicted in Fig. 1.

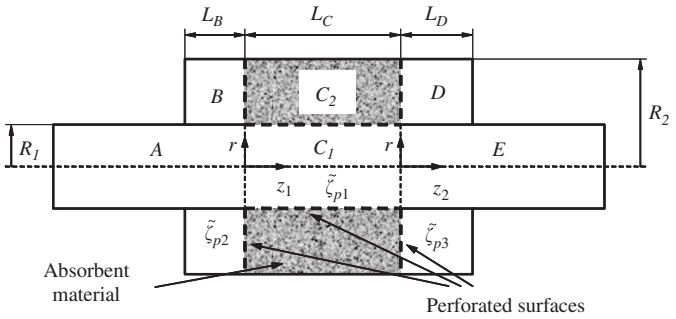

Fig. 1. Perforated dissipative circular muffler with empty extended ducts.

2.1. Wave propagation in regions A and E

The solution of the Helmholtz equation may be expressed for the extended inlet A (and duct E) as [3]

$$P_A(r, z_1) = \sum_{n=0}^{\infty} (A_n^+ \mathrm{e}^{-\mathrm{j}k_{z,A,n}z_1} + A_n^- \mathrm{e}^{\mathrm{j}k_{z,A,n}z_1}) \psi_{A,n}(r), \tag{1}$$

where $\mathrm{j} = \sqrt{-1}$ is the imaginary unit, n the mode number, (r, z_1) the cylindrical coordinates, and A_n^+, A_n^- the wave propagation coefficients. Here $\psi_{A,n}(r)$ is the eigenfunction for the duct, given by the zeroth-order Bessel function of the first kind $J_0(k_{r,A,n}r)$, where the radial wavenumber $k_{r,A,n}$ satisfies the rigid wall boundary condition. The axial wavenumber $k_{z,A,n}$ of the mode n is given by

$$k_{z,A,n}^2 = k_0^2 - k_{r,A,n}^2, \tag{2}$$

with $k_0 = \omega/c_0$ being the wavenumber in air and ω the angular frequency. The acoustic velocity in z direction in region A may be written, using Eq. (1) and the linearized momentum equation [1], to give

$$U_A(r, z_1) = \frac{1}{\rho_0 \omega} \sum_{n=0}^{\infty} k_{z,A,n} (A_n^+ \mathrm{e}^{-\mathrm{j}k_{z,A,n}z_1} - A_n^- \mathrm{e}^{\mathrm{j}k_{z,A,n}z_1}) \psi_{A,n}(r). \tag{3}$$

2.2. Wave propagation in regions B and D

In the case of the annular duct B (and D), a solution of the Helmholtz equation is assumed in the form [3]

$$P_B(r, z_1) = \sum_{n=0}^{\infty} (B_n^+ \mathrm{e}^{-\mathrm{j}k_{z,B,n}z_1} + B_n^- \mathrm{e}^{\mathrm{j}k_{z,B,n}z_1}) \psi_{B,n}(r), \tag{4}$$

B_n^+ and B_n^- being the wave propagation coefficients and $\psi_{B,n}(r)$ the eigenfunction given by

$$\psi_{B,n}(r) = J_0(k_{r,B,n}r) - \frac{J_1(k_{r,B,n}R_2)}{Y_1(k_{r,B,n}R_2)} Y_0(k_{r,B,n}r). \tag{5}$$

Here, J_1 is the first-order Bessel function of the first kind, Y_0 and Y_1 are the zeroth- and first-order Bessel functions of the second kind, respectively, and $k_{r,B,n}$ is the radial wavenumber satisfying the rigid wall boundary condition in the inner and outer annulus walls. The axial wavenumber $k_{z,B,n}$ can be obtained from

$$k_{z,B,n}^2 = k_0^2 - k_{r,B,n}^2, \tag{6}$$

and the axial velocity is given by

$$U_B(r,z_1)=\frac{1}{\rho_0\omega}\sum_{n=0}^{\infty}k_{z,B,n}(B_n^+\mathrm{e}^{-\mathrm{j}k_{z,B,n}z_1}-B_n^-\mathrm{e}^{\mathrm{j}k_{z,B,n}z_1})\psi_{B,n}(r). \tag{7}$$

2.3. Wave propagation in region C

In region C, the acoustic pressure is written as [14]

$$P_C(r,z_1)=\sum_{n=0}^{\infty}(C_n^+\mathrm{e}^{-\mathrm{j}k_{z,C,n}z_1}+C_n^-\mathrm{e}^{\mathrm{j}k_{z,C,n}z_1})\psi_{C,n,P}(r), \tag{8}$$

which can be divided into two parts as

$$P_C(r,z_1)=\begin{cases}P_{C_1}(r,z_1), & 0\leqslant r\leqslant R_1,\\ P_{C_2}(r,z_1), & R_1\leqslant r\leqslant R_2,\end{cases} \tag{9}$$

for the central inner duct and the sound-absorbing material, respectively. In addition, the transversal pressure eigenfunction is given by

$$\psi_{C,n,P}(r)=\begin{cases}\psi_{C_1,n,P}(r), & 0\leqslant r\leqslant R_1,\\ \psi_{C_2,n,P}(r), & R_1\leqslant r\leqslant R_2.\end{cases} \tag{10}$$

The central inner duct and outer chamber with absorbing material have the same axial wavenumber $k_{z,C,n}$, which is related to the radial wavenumber of the air $k_{r,C,n}$ and fiber $\tilde{k}_{r,C,n}$ through

$$k_{z,C,n}^2=k_0^2-k_{r,C,n}^2, \tag{11}$$

$$k_{z,C,n}^2=\tilde{k}^2-\tilde{k}_{r,C,n}^2. \tag{12}$$

The wavenumbers and the eigenfunctions can be evaluated from the conditions to be satisfied by the acoustic field, as established in Refs. [11,14]. These conditions are: (1) the pressure is finite at $r=0$; (2) the radial velocity is zero at $r=R_2$; (3) the radial velocity is continuous across the perforated duct with $r=R_1$; and (4) the perforated screen leads to an acoustic pressure difference that can be expressed by

$$P_{C_1}(r,z_1)-P_{C_2}(r,z_1)=\rho_0c_0\tilde{\zeta}_{p1}U_r,\quad r=R_1, \tag{13}$$

U_r being the radial acoustic velocity at the perforated surface. The foregoing four conditions yield the characteristic equation and the eigenfunctions. The former can be written as

$$\frac{\rho_0\tilde{k}_{r,C,n}}{\tilde{\rho}k_{r,C,n}}\left(\frac{J_0(k_{r,C,n}R_1)}{J_1(k_{r,C,n}R_1)}+\frac{\mathrm{j}\tilde{\zeta}_{p1}k_{r,C,n}}{k_0}\right)=\frac{J_0(\tilde{k}_{r,C,n}R_1)Y_1(\tilde{k}_{r,C,n}R_2)-Y_0(\tilde{k}_{r,C,n}R_1)J_1(\tilde{k}_{r,C,n}R_2)}{J_1(\tilde{k}_{r,C,n}R_1)Y_1(\tilde{k}_{r,C,n}R_2)-Y_1(\tilde{k}_{r,C,n}R_1)J_1(\tilde{k}_{r,C,n}R_2)}, \tag{14}$$

which is solved in combination with Eqs. (11) and (12) to obtain the axial wavenumbers. Details of an iterative solution technique can be found in Ref. [14]. Finally, the transversal pressure eigenfunctions in region C are given by

$$\psi_{C,n,P}(r)=\begin{cases}J_0(k_{r,C,n}r), & 0\leqslant r\leqslant R_1,\\ F\left(J_0(\tilde{k}_{r,C,n}r)-\dfrac{J_1(\tilde{k}_{r,C,n}R_2)}{Y_1(\tilde{k}_{r,C,n}R_2)}Y_0(\tilde{k}_{r,C,n}r)\right), & R_1\leqslant r\leqslant R_2,\end{cases} \tag{15}$$

with

$$F=\left(J_0(k_{r,C,n}R_1)+\frac{\mathrm{j}\tilde{\zeta}_{p1}k_{r,C,n}}{k_0}J_1(k_{r,C,n}R_1)\right)\frac{Y_1(\tilde{k}_{r,C,n}R_2)}{J_0(\tilde{k}_{r,C,n}R_1)Y_1(\tilde{k}_{r,C,n}R_2)-J_1(\tilde{k}_{r,C,n}R_2)Y_0(\tilde{k}_{r,C,n}R_1)}. \tag{16}$$

In view of the linearized momentum equation and Eqs. (8) and (15), the axial velocity in region C may be expressed as

$$U_C(r,z_1)=\frac{1}{\rho_0\omega}\sum_{n=0}^{\infty}k_{z,C,n}(C_n^+\mathrm{e}^{-\mathrm{j}k_{z,C,n}z_1}-C_n^-\mathrm{e}^{\mathrm{j}k_{z,C,n}z_1})\psi_{C,n,U}(r) \tag{17}$$

with the transversal velocity eigenfunction given by

$$\psi_{C,n,U}(r)=\begin{cases}J_0(k_{r,C,n}r), & 0\leqslant r\leqslant R_1,\\ F\dfrac{\rho_0}{\tilde{\rho}}\left(J_0(\tilde{k}_{r,C,n}r)-\dfrac{J_1(\tilde{k}_{r,C,n}R_2)}{Y_1(\tilde{k}_{r,C,n}R_2)}Y_0(\tilde{k}_{r,C,n}r)\right), & R_1\leqslant r\leqslant R_2.\end{cases} \tag{18}$$

2.4. Evaluation of the wave coefficients

Once the expressions for the acoustic pressure and velocity have been established, the unknown wave coefficients can be evaluated by applying the axial matching conditions. Considering the muffler depicted earlier in Fig. 1, the conditions of the acoustic pressure and velocity at $z_1=0$ (expansion) are

$$P_A|_{z_1=0}=P_C|_{z_1=0}\quad \text{for } 0\leqslant r\leqslant R_1, \tag{19}$$

$$P_B|_{z_1=0}-P_C|_{z_1=0}=\rho_0c_0\tilde{\zeta}_{p2}U_B|_{z_1=0}\quad \text{for } R_1\leqslant r\leqslant R_2, \tag{20}$$

$$U_C|_{z_1=0}=\begin{cases}U_A|_{z_1=0} & \text{for } 0\leqslant r\leqslant R_1,\\ U_B|_{z_1=0} & \text{for } R_1\leqslant r\leqslant R_2.\end{cases} \tag{21}$$

Note that Eq. (20) accounts for the effect of a perforated screen, relating the acoustic pressure difference between regions B and C with the acoustic impedance and the axial acoustic velocity. For the left end rigid plate, the velocity condition is

$$U_B|_{z_1=-L_B}=0\quad \text{for } R_1\leqslant r\leqslant R_2 \tag{22}$$

and, in view of the orthogonality of the eigenfunction [3] this yields

$$B_n^+=B_n^-\mathrm{e}^{-2\mathrm{j}k_{z,B,n}L_B}. \tag{23}$$

Similarly, at $z_1=L_C$ and $z_2=0$ (contraction),

$$P_E|_{z_2=0}=P_C|_{z_1=L_C}\quad \text{for } 0\leqslant r\leqslant R_1, \tag{24}$$

$$P_C|_{z_1=L_C}-P_D|_{z_2=0}=\rho_0c_0\tilde{\zeta}_{p3}U_D|_{z_2=0}\quad \text{for } R_1\leqslant r\leqslant R_2, \tag{25}$$

$$U_C|_{z_1=L_C}=\begin{cases}U_E|_{z_2=0} & \text{for } 0\leqslant r\leqslant R_1,\\ U_D|_{z_2=0} & \text{for } R_1\leqslant r\leqslant R_2.\end{cases} \tag{26}$$

Finally, at the right wall of the muffler

$$U_D|_{z_2=L_D}=0\quad \text{for } R_1\leqslant r\leqslant R_2, \tag{27}$$

thus giving

$$D_n^-=D_n^+\mathrm{e}^{-2\mathrm{j}k_{z,D,n}L_D}. \tag{28}$$

The calculation of the wave coefficients requires the generation of a suitable system of equations. A number of integration procedures can be considered [13,14,19,20] to obtain the solution to Eqs. (19)–(21) and (24)–(26). One approach consists of truncating the number of modes to a suitable value N, and then integrating Eqs. (19)–(21) and (24)–(26) directly over discrete zones at the geometrical discontinuities. This direct integration (DI) procedure, as elaborated in Appendix A, was shown to be effective in dissipative chambers without extensions [13,14], with the integrals carried out along the radius.

An alternative to the foregoing DI approach is the standard mode-matching method, which uses a weighted integration (WI) over the whole cross-sectional area [19], with the weighting functions being the transverse modes of the ducts. For the expansion, the integral associated with the pressure continuity, Eq. (19), may then be expressed as

$$\sum_{n=0}^{N}(A_n^+ + A_n^-)\int_0^{R_1}\psi_{A,n}(r)\psi_{A,s}(r)r\,\mathrm{d}r = \sum_{n=0}^{N}(C_n^+ + C_n^-)\int_0^{R_1}\psi_{C,n,P}(r)\psi_{A,s}(r)r\,\mathrm{d}r, \tag{29}$$

where $s = 0, 1, \ldots, N$. The integration of Eq. (20) yields

$$\begin{aligned}&\sum_{n=0}^{N}B_n^-(\mathrm{e}^{-2\mathrm{j}k_{z,B,n}L_B}+1)\int_{R_1}^{R_2}\psi_{B,n}(r)\psi_{B,s}(r)r\,\mathrm{d}r - \sum_{n=0}^{N}(C_n^+ + C_n^-)\int_{R_1}^{R_2}\psi_{C,n,P}(r)\psi_{B,s}(r)r\,\mathrm{d}r\\ &\quad = \frac{c_0\tilde{\zeta}_{p2}}{\omega}\sum_{n=0}^{N}k_{z,B,n}B_n^-(\mathrm{e}^{-2\mathrm{j}k_{z,B,n}L_B}-1)\int_{R_1}^{R_2}\psi_{B,n}(r)\psi_{B,s}(r)r\,\mathrm{d}r,\end{aligned} \tag{30}$$

and the integration of the velocity conditions given by Eq. (21) leads to

$$\begin{aligned}&\sum_{n=0}^{N}k_{z,C,n}(C_n^+ - C_n^-)\int_0^{R_2}\psi_{C,n,U}(r)\psi_{C,s,P}(r)r\,\mathrm{d}r = \sum_{n=0}^{N}k_{z,A,n}(A_n^+ - A_n^-)\int_0^{R_1}\psi_{A,n}(r)\psi_{C,s,P}(r)r\,\mathrm{d}r\\ &\quad + \sum_{n=0}^{N}k_{z,B,n}B_n^-(\mathrm{e}^{-2\mathrm{j}k_{z,B,n}L_B}-1)\int_{R_1}^{R_2}\psi_{B,n}(r)\psi_{C,s,P}(r)r\,\mathrm{d}r.\end{aligned} \tag{31}$$

Note that in Eq. (31) the mode $\psi_{C,s,P}(r)$ is used as a weighting function to retain orthogonality [21] on the left-hand side (the difference between $\psi_{C,s,P}(r)$ and $\psi_{C,s,U}(r)$ is the term $\rho_0/\tilde{\rho}$). For the contraction, similar equations are obtained. The integrations of Eqs. (24)–(26) respectively yield

$$\begin{aligned}&\sum_{n=0}^{N}(E_n^+ + E_n^-)\int_0^{R_1}\psi_{E,n}(r)\psi_{E,s}(r)r\,\mathrm{d}r\\ &\quad = \sum_{n=0}^{N}(C_n^+\mathrm{e}^{-\mathrm{j}k_{z,C,n}L_C} + C_n^-\mathrm{e}^{\mathrm{j}k_{z,C,n}L_C})\int_0^{R_1}\psi_{C,n,P}(r)\psi_{E,s}(r)r\,\mathrm{d}r,\end{aligned} \tag{32}$$

$$\begin{aligned}&\sum_{n=0}^{N}(C_n^+\mathrm{e}^{-\mathrm{j}k_{z,C,n}L_C} + C_n^-\mathrm{e}^{\mathrm{j}k_{z,C,n}L_C})\int_{R_1}^{R_2}\psi_{C,n,P}(r)\psi_{D,s}(r)r\,\mathrm{d}r\\ &\quad - \sum_{n=0}^{N}D_n^+(1+\mathrm{e}^{-2\mathrm{j}k_{z,D,n}L_D})\int_{R_1}^{R_2}\psi_{D,n}(r)\psi_{D,s}(r)r\,\mathrm{d}r\\ &\quad = \frac{c_0\tilde{\zeta}_{p3}}{\omega}\sum_{n=0}^{N}k_{z,D,n}D_n^+(1-\mathrm{e}^{-2\mathrm{j}k_{z,D,n}L_D})\int_{R_1}^{R_2}\psi_{D,n}(r)\psi_{D,s}(r)r\,\mathrm{d}r,\end{aligned} \tag{33}$$

$$\begin{aligned}&\sum_{n=0}^{N}k_{z,C,n}(C_n^+\mathrm{e}^{-\mathrm{j}k_{z,C,n}L_C} - C_n^-\mathrm{e}^{\mathrm{j}k_{z,C,n}L_C})\int_0^{R_2}\psi_{C,n,U}(r)\psi_{C,s,P}(r)r\,\mathrm{d}r\\ &\quad = \sum_{n=0}^{N}k_{z,E,n}(E_n^+ - E_n^-)\int_0^{R_1}\psi_{E,n}(r)\psi_{C,s,P}(r)r\,\mathrm{d}r\\ &\quad + \sum_{n=0}^{N}k_{z,D,n}D_n^+(1-\mathrm{e}^{-2\mathrm{j}k_{z,D,n}L_D})\int_{R_1}^{R_2}\psi_{D,n}(r)\psi_{C,s,P}(r)r\,\mathrm{d}r,\end{aligned} \tag{34}$$

with $s = 0, 1, \ldots, N$. The integrals involved in Eqs. (29)–(34) can be analytically evaluated as [22]

$$\int_0^{r_0} B_0(\lambda r) C_0(\mu r) r \, \mathrm{d}r = \begin{cases} \dfrac{r_0}{\lambda^2 - \mu^2}(\lambda B_1(\lambda r) C_0(\mu r) - \mu B_0(\lambda r) C_1(\mu r)), & \lambda \neq \mu, \\ \dfrac{r_0^2}{2}(B_0(\lambda r) C_0(\lambda r) + B_1(\lambda r) C_1(\lambda r)), & \lambda = \mu, \end{cases} \tag{35}$$

with B_0, C_0 and B_1, C_1 being the Bessel functions of any kind, and zeroth- and first-order, respectively.

To determine the acoustic attenuation performance of the muffler, the transmission loss can be evaluated. If the values $A_0^+ = 1$, $A_n^+ = 0$, $n > 0$ (incident plane wave) and $E_n^- = 0$ for $n = 0, 1, 2, \ldots$ (anechoic termination) are assumed, the system defined by Eqs. (29)–(34) provides a set of 6 $(N+1)$ equations with 6 $(N+1)$ unknowns (A_n^-, B_n^-, C_n^+, C_n^-, D_n^+ and E_n^+). Once these values are solved, the transmission loss is evaluated as

$$\mathrm{TL} = -20 \log_{10} |E_0^+|. \tag{36}$$

3. Results and discussion

The configurations considered in the study are shown in Table 1. Geometries 1–4 are defined by $R_1 = 0.0268\,\mathrm{m}$, $R_2 = 0.0886\,\mathrm{m}$, and $L = L_B + L_C + L_D = 0.2\,\mathrm{m}$, corresponding to the prototype fabricated to carry out the experimental measurements. For these geometries, different lengths of the extended inlet and outlet ducts are considered. These lengths are chosen to cover a broad range of possible configurations: $L_B = L_D = 0\,\mathrm{m}$, no extensions, geometry 1; $L_B = 0.087\,\mathrm{m}$, $L_D = 0.037\,\mathrm{m}$, optimal extensions for a reactive chamber [3], geometry 2; $L_B = 0.075\,\mathrm{m}$, $L_D = 0.025\,\mathrm{m}$, shorter extensions than the optimal case, geometry 3; and $L_B = 0.1\,\mathrm{m}$, $L_D = 0.05\,\mathrm{m}$, longer extensions than the optimal configuration, geometry 4. To illustrate the behavior of larger mufflers, geometries 5–7 have a larger chamber radius, defined by $R_2 = 0.1772\,\mathrm{m}$, and the axial lengths are also modified: $L_B = 0.075\,\mathrm{m}$, $L_C = 0.1\,\mathrm{m}$, $L_D = 0.025\,\mathrm{m}$, geometry 5 (similar to geometry 3); $L_B = 0.15\,\mathrm{m}$, $L_C = 0.2\,\mathrm{m}$, $L_D = 0.05\,\mathrm{m}$, geometry 6 (twice the values of geometry 3); and $L_B = 0.3\,\mathrm{m}$, $L_C = 0.4\,\mathrm{m}$, $L_D = 0.1\,\mathrm{m}$, geometry 7 (four times the values of geometry 3). For the absorbing material considered in the present work, the complex values of the characteristic impedance $\tilde{Z} = \tilde{\rho}\tilde{c}$ and wavenumber $\tilde{k} = \omega/\tilde{c}$ are given by [18]

$$\tilde{Z} = Z_0 \left[\left(1 + 0.09534 \left(\frac{f\rho_0}{R} \right)^{-0.754} \right) + \mathrm{j} \left(-0.08504 \left(\frac{f\rho_0}{R} \right)^{-0.732} \right) \right], \tag{37}$$

$$\tilde{k} = k_0 \left[\left(1 + 0.16 \left(\frac{f\rho_0}{R} \right)^{-0.577} \right) + \mathrm{j} \left(-0.18897 \left(\frac{f\rho_0}{R} \right)^{-0.595} \right) \right], \tag{38}$$

where $Z_0 = \rho_0 c_0$ is the characteristic impedance of air, f is the frequency, and R is the steady airflow resistivity: 4896 or 17378 rayl/m for bulk densities of 100 or 200 $\mathrm{kg/m^3}$, respectively. The dimensionless perforate acoustic impedance $\tilde{\zeta}_p$ used in Eqs. (13), (20), and (25) establishes the relationship between the acoustic pressure drop

Table 1
Geometry of perforated dissipative mufflers with empty extensions

Geometry	R_1 (m)	R_2 (m)	L_B (m)	L_C (m)	L_D (m)
1	0.0268	0.0886	0.0	0.2	0.0
2	0.0268	0.0886	0.087	0.076	0.037
3	0.0268	0.0886	0.075	0.1	0.025
4	0.0268	0.0886	0.1	0.05	0.05
5	0.0268	0.1772	0.075	0.1	0.025
6	0.0268	0.1772	0.15	0.2	0.05
7	0.0268	0.1772	0.3	0.4	0.1

and the normal acoustic velocity through the interface. The acoustic impedance in the absence of absorbing material is given by [23,24]

$$\zeta_p = \frac{0.006 + \mathrm{j}k_0(t_p + 0.85d_h F(\sigma))}{\sigma}, \tag{39}$$

with d_h denoting the hole diameter, t_p the thickness, σ the porosity, and $F(\sigma)$ a function that accounts for the interaction between holes. Here, $F(\sigma)$ is obtained as the average value of Ingard's and Fok's corrections [24], denoted as $F_I(\sigma)$ and $F_F(\sigma)$, respectively. Ingard's function is given by

$$F_I(\sigma) = 1 - 0.7\sqrt{\sigma}, \tag{40}$$

and Fok's correction is written as

$$F_F(\sigma) = 1 - 1.41\sqrt{\sigma} + 0.34(\sqrt{\sigma})^3 + 0.07(\sqrt{\sigma})^5. \tag{41}$$

To incorporate the effect of the absorbing material, Eq. (39) has been modified to [18,25]

$$\tilde{\zeta}_p = \frac{0.006 + \mathrm{j}k_0(t_p + 0.425d_h(1 + (\tilde{Z}/Z_0)(\tilde{k}/k_0))F(\sigma))}{\sigma}. \tag{42}$$

The properties of the perforated surfaces will be specified later in Section 3.4.

First, the analytical methodology is compared with FE calculations, and both the analytical and numerical modeling techniques are also validated with experimental results for a selected configuration. Then, the effect of extension lengths, resistivity of the absorbing material, porosity of the perforated screens, and muffler dimensions is investigated in detail. A comparison between DI and WI approaches is given in Appendix B.

3.1. Validation

Fig. 2 shows the transmission loss of the dissipative muffler with empty inlet/outlet extensions associated with geometry 3. Comparison is given between the DI (radius and area integrals) and WI procedures for $N = 13$ (14 modes). Also included for validation purposes are the FE solution and an experimental measurement. A value of $R = 4896$ rayl/m is considered, and no perforated surfaces are included. The porosity of the perforated surfaces in the experimental measurement depicted is very high (over 80%), and therefore the values $\tilde{\zeta}_{p1} = \tilde{\zeta}_{p2} = \tilde{\zeta}_{p3} = 0$ have been used in the computations. Analytical results and FEM calculations show an excellent agreement, although the DI approach exhibits slight discrepancies close to 1600 Hz even when the solutions chosen have a very low error (see Appendix B, Fig. B1(b), DI radius and DI area with 14 modes). In addition, experimental measurements are included that demonstrate the accuracy of the models for practical purposes. Therefore, the WI approach is selected for the analysis of the acoustic attenuation performance of perforated dissipative mufflers with empty inlet/outlet extensions, which is presented in the following sections.

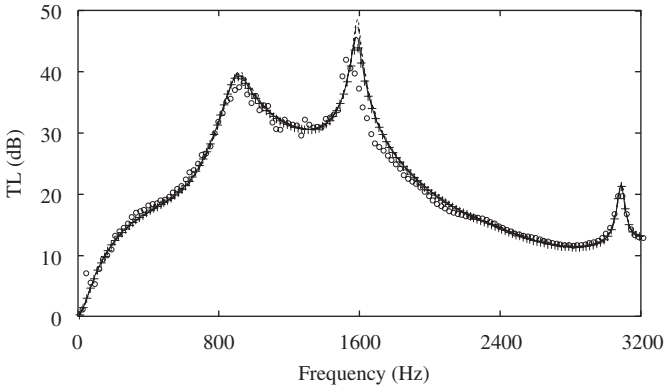

Fig. 2. Transmission loss of dissipative muffler with empty inlet/outlet extensions, geometry 3 and $R = 4896$ rayl/m: ——, WI; - - - -, DI, radius; – – –, DI, area; + + +, FEM; ○○○, experimental.

3.2. Effect of extensions

The lengths considered in this section for the muffler with empty extended inlet/outlet ducts are those detailed in Table 1, which are chosen to show the effect of arbitrary lengths, such as geometries 3 and 4, as well as theoretically suitable extended ducts (geometry 2) for a chamber without absorbing material [3,4]. In addition, similar dissipative mufflers with absorbent-filled inlet/outlet extensions are also considered [19] to examine the effect of removing absorbent from the extensions. Geometry 1 is a fully filled dissipative muffler without extensions which has been included in the analysis for comparison purposes. A value of $R = 2000$ rayl/m is considered for all the configurations including fiber, and no perforated surfaces are taken into account in this section.

Fig. 3 shows the TL of geometry 3 obtained by means of the WI analytical approach presented in this work, as well as the TL of the same geometry completely filled with absorbing material [19] and without fiber [3]. A fully filled dissipative muffler without extensions associated with geometry 1 is also considered to compare the acoustic performance. At low and mid frequencies, the dissipative muffler with empty inlet/outlet extensions exhibits an attenuation with some resemblance to that related to the reactive chamber, retaining the quarter-wave resonance. The presence of absorbing material in the central part of the muffler eliminates the pass bands, thus leading to a better acoustic behavior, and introduces some damping and a slight frequency shift at the maximum attenuation. At higher frequencies, the collapse of the TL associated with the reactive chamber is evident, whereas the muffler with empty extensions partially retains the good acoustic properties of dissipative silencers at high frequencies. As far as the absorbent-filled extended inlet/outlet muffler is concerned, its behavior deviates from that observed in the configuration with empty extensions, since the primary resonance peak is essentially eliminated. A higher attenuation appears close to 1600 Hz, although the prediction of this behavior is not as intuitive as in the case of the empty extensions, in which the peaks are close to those of a purely reactive muffler. At higher frequencies, the attenuation is better in the case of the absorbent-filled extensions, since this geometry includes more absorbing material. Regarding the dissipative muffler without extensions (geometry 1), its behavior is clearly worse in the low and mid frequency range in comparison with the other dissipative configurations, since the participation of resonances is excluded. For higher frequencies, however, the acoustic performance is better. The intersection of TL between this muffler and the empty inlet/outlet geometry is approximately at 1800 Hz.

A similar analysis can be carried out from the results depicted in Fig. 4 for geometry 2. The extensions are now selected so that the reactive geometry exhibits a broadband attenuation dome without pass bands [3], at least before the propagation of higher-order modes. In this case, the dissipative muffler with empty extensions, as well as the absorbent-filled configuration, reproduce this behavior, with a slight advantage in the former case in the mid frequency range, due to a resonance close to 800 Hz. For higher frequencies, both geometries are better than the reactive configuration, as expected. Since the extended lengths are now longer than in

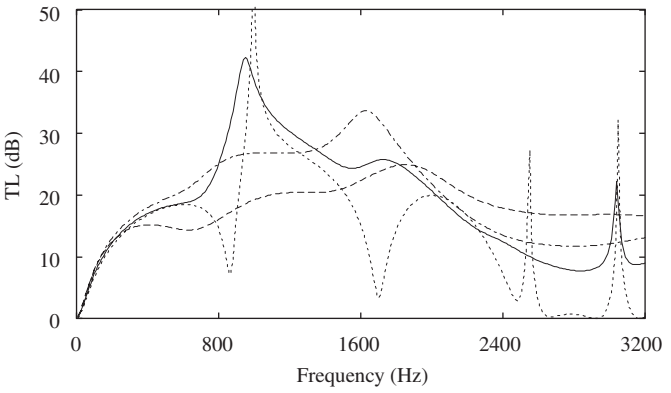

Fig. 3. Transmission loss of dissipative mufflers, $R = 2000$ rayl/m: ——, geometry 3, empty extensions; – – – –, geometry 3, absorbent-filled extensions; - - - -, geometry 3, no fiber; – – –, geometry 1, fully filled, no extensions.

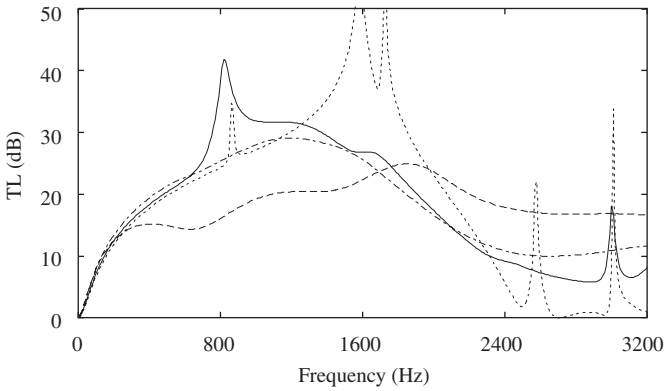

Fig. 4. Transmission loss of dissipative mufflers, $R = 2000$ rayl/m: ——, geometry 2, empty extensions; – – – –, geometry 2, absorbent-filled extensions; - - - -, geometry 2, no fiber; – – –, geometry 1, fully filled, no extensions.

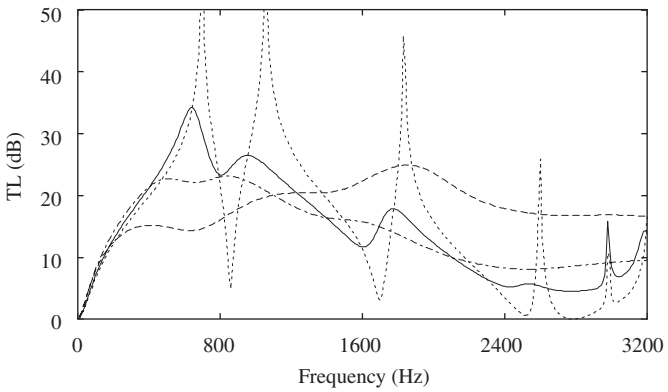

Fig. 5. Transmission loss of dissipative mufflers, $R = 2000$ rayl/m: ——, geometry 4, empty extensions; – – – –, geometry 4, absorbent-filled extensions; - - - -, geometry 4, no fiber; – – –, geometry 1, fully filled, no extensions.

geometry 3, the amount of fiber in the case of the muffler with empty extensions is reduced, leading to a lower attenuation for higher frequencies in comparison with Fig. 3.

For longer extensions (geometry 4), as those considered in Fig. 5, the comments associated with Fig. 3 are also valid with some remarks. The empty extensions configuration still exhibits the best acoustic performance among the dissipative mufflers for low frequencies. The intersection of TL between the fully filled configuration without extensions (geometry 1) and empty extensions configuration (geometry 4) is now at 1260 Hz, whereas in Fig. 3 this value was 1800 Hz between geometries 1 and 3. The empty extensions of geometry 4 are longer than those of geometries 2 and 3, and therefore the length of the central part with fiber is shorter in the case of geometry 4. This leads to a lower attenuation in the high-frequency range for the empty extensions configuration of Fig. 5 in comparison with Figs. 3 and 4. Geometry 4 with absorbent-filled extensions also suffers this detrimental effect for longer extensions, as it has been observed by Selamet et al. [19]. At high frequencies, the behavior of mufflers with empty and absorbent-filled extensions is better than in the case of the purely reactive chamber, except for some narrow frequency bands associated with resonant peaks.

3.3. *Effect of resistivity*

The effect of the flow resistivity for the values $R = 1000$, 2000 and 4896 rayl/m is analyzed in Figs. 6 and 7, for geometries 2 ($L_B = 0.087$ m, $L_D = 0.037$ m) and 4 ($L_B = 0.1$ m, $L_D = 0.05$ m), respectively, with empty

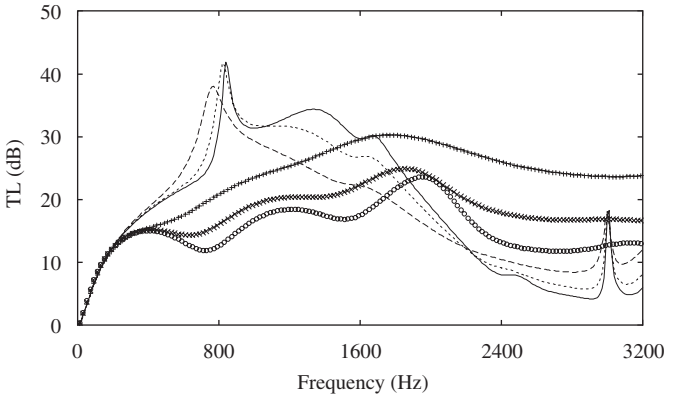

Fig. 6. Transmission loss of dissipative mufflers: ——, geometry 2, $R = 1000$ rayl/m; - - - -, geometry 2, $R = 2000$ rayl/m; – – –, geometry 2, $R = 4896$ rayl/m; ○○○, geometry 1, $R = 1000$ rayl/m; × × ×, geometry 1, $R = 2000$ rayl/m; + + +, geometry 1, $R = 4896$ rayl/m.

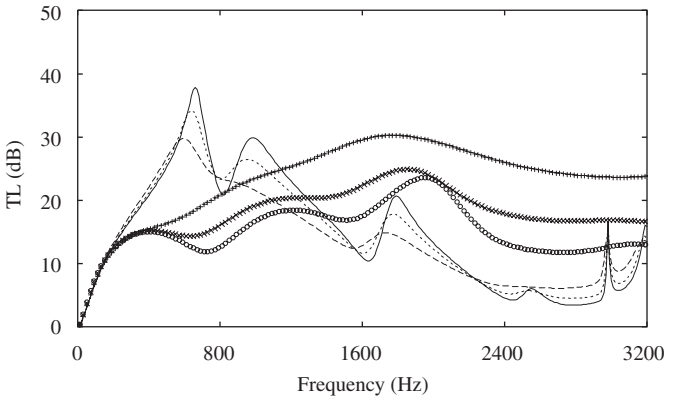

Fig. 7. Transmission loss of dissipative mufflers: ——, geometry 4, $R = 1000$ rayl/m; - - - -, geometry 4, $R = 2000$ rayl/m; – – –, geometry 4, $R = 4896$ rayl/m; ○○○, geometry 1, $R = 1000$ rayl/m; × × ×, geometry 1, $R = 2000$ rayl/m; + + +, geometry 1, $R = 4896$ rayl/m.

extensions. In both cases, comparison is given with the TL associated with geometry 1 and the same resistivities. The values $\tilde{\zeta}_{p1} = \tilde{\zeta}_{p2} = \tilde{\zeta}_{p3} = 0$ have been used in all the analytical computations.

From Fig. 6, the effect of the fiber resistivity is very clear. With empty extensions (geometry 2), the behavior is improved in the mid frequency range as the resistivity is reduced, and the peaks associated with resonances shift to lower frequencies for higher resistivities. The opposite trend is true in the high-frequency range, where higher resistivities lead to increased attenuation. For geometry 1 (no extensions), the behavior is basically improved as the resistivity increases. Comparing both geometries, it may be concluded that empty extensions enable to obtain a better acoustic performance in the mid frequency range, mainly for low resistivities. As the resistivity of the absorbing material becomes higher, this advantage of the geometry with empty extensions is gradually lost. For longer extensions (Fig. 7), such as those of geometry 4, the amount of fiber is reduced in the central part of the muffler with empty extensions. Therefore, geometry 4 keeps its dominance for low frequencies, but the performance of geometry 1 becomes better earlier (lower frequencies) than in Fig. 6. The frequencies at which the TL of both geometries intercept are reduced as the resistivity is increased.

3.4. Effect of perforated surfaces

The effect of perforated surfaces on the acoustic attenuation performance of mufflers with empty extensions is shown in Fig. 8 for geometry 3 and $R = 4896$ rayl/m. The perforations have $d_h = 0.0035$ m and

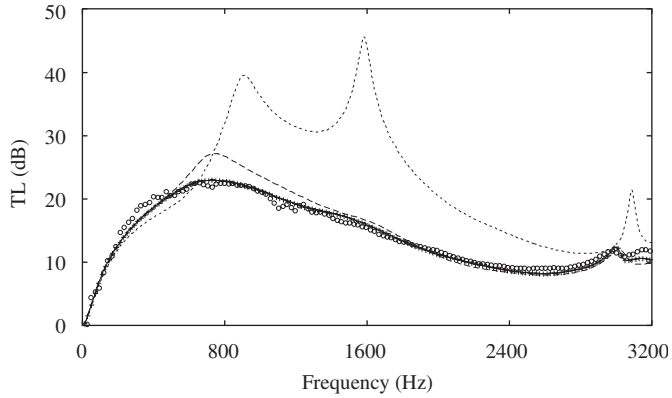

Fig. 8. Transmission loss of dissipative muffler with empty inlet/outlet extensions, geometry 3 and $R = 4896$ rayl/m: ----, 100% open; – – –, perforated central pipe, $\sigma = 11\%$; ——, perforated central pipe and plates, $\sigma = 11\%$; + + +, perforated central pipe and plates, $\sigma = 11\%$, FEM; ○○○, perforated central pipe and plates, $\sigma = 11\%$, experimental.

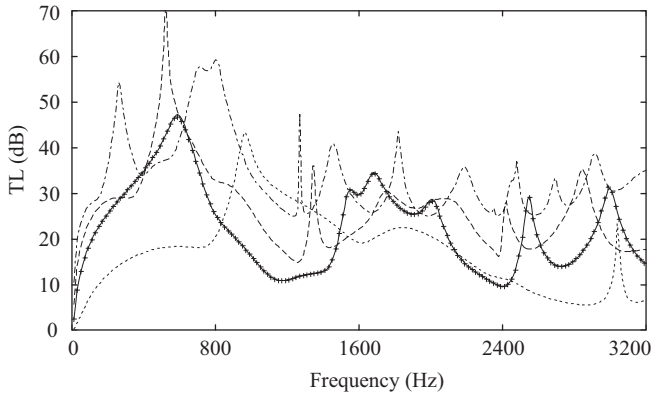

Fig. 9. Transmission loss of dissipative mufflers with empty inlet/outlet extensions, $R = 1000$ rayl/m: ----, geometry 3; ——, geometry 5; + + +, same, FEM; – – –, geometry 6; – – – –, geometry 7.

$t_p = 0.0003$ m and the porosity is $\sigma = 11\%$. For this value of porosity, two configurations are analyzed, the former with only a perforated central duct and fully open lateral plates, and the latter with perforated central duct and plates. In addition to the analytical results, FEM calculations and experimental measurements are included for the configuration with perforated central duct and lateral surfaces, to provide validation. A reduction of the porosity leads to detrimental effect in the acoustic attenuation performance, with the exception of low frequencies, similar to the results found in other muffler geometries [16,19]. Above 800 Hz, the best attenuation is obtained by the muffler without perforated interface, followed by the configuration with only a central perforated pipe and fully open lateral plates. The addition of perforated end plates produces a lower attenuation in the mid frequency range, although the behavior is similar at high frequencies.

3.5. *Effect of muffler dimensions*

Results for larger dissipative mufflers with empty inlet/outlet extensions are presented in Fig. 9, while retaining geometry 3 for comparison purposes. The chamber radius $R_2 = 0.1772$ m associated with geometries 5–7 is twice the value of geometry 3, therefore promoting the participation of higher order modes. To reduce the attenuation of these modes, the resistivity of the absorbing material is low, with a value $R = 1000$ rayl/m. Different axial lengths are also considered: for geometries 3 and 5, the same values are taken into account,

given by $L_B = 0.075\,\text{m}$, $L_C = 0.1\,\text{m}$ and $L_D = 0.025\,\text{m}$. For geometry 6 these values are multiplied by a factor of 2, and for geometry 7 a factor of 4 is considered. The values $\tilde{\zeta}_{p1} = \tilde{\zeta}_{p2} = \tilde{\zeta}_{p3} = 0$ have been used in all the calculations.

At low frequencies, the attenuation of geometries 5–7 is clearly better than in the case of geometry 3, since the radius R_2 has been doubled. In this frequency range, the first attenuation peak of the larger mufflers exhibits a shift towards lower frequencies as the length of the extended ducts is increased. The effect of the higher-order modes is more important for larger mufflers, as can be observed in the figure, where the shape of the TL becomes more irregular and a higher number of peaks can be found as the radius is increased. This effect is also evident by comparing the frequency of the first attenuation peak for geometries 3 and 5. In the former, this frequency is dictated by the axial resonance associated with the extended duct B. In the latter, however, this frequency is lower, even when the length of duct B is the same, due to the propagation of the first higher-order mode. This multidimensional propagation is properly predicted by the models, as can be inferred from the good agreement between the analytical and FE calculations for geometry 5. Finally, at high frequencies the attenuation is dictated in general by the presence of absorbing material. Hence, the increase of the radius and/or the dissipative chamber length L_C leads to a higher TL.

4. Conclusions

The acoustic behavior of perforated dissipative mufflers with empty extended inlet/outlet has been investigated in detail by means of a 2D axisymmetric analytical approach and the FEM. Both approaches are complementary, and the study has provided an opportunity to benchmark one against the other and also against experimental measurements. To generate an algebraic system of equations from the continuity conditions of the acoustic field in the axial direction, two procedures (DI and WI) have been presented and discussed. A benchmark with FE results shows that both analytical approaches work properly with geometries without extensions. The performance of DI procedure, however, is reduced in terms of convergence speed in the presence of extended ducts and therefore, the WI approach has been selected. Both the analytical (WI) and numerical (FE) modeling techniques have been compared with experiments for selected configurations, providing a validation for practical purposes. Several effects have been studied, including the influence of the inlet/outlet lengths, fiber resistivity, porosity of the perforated surfaces, and muffler dimensions. The use of empty extensions provides a suitable method for controlling the quarter-wave resonator frequencies, which leads to a desirable acoustic performance of the muffler at low and mid frequencies. In comparison with fully filled dissipative mufflers, the empty extensions are observed to lead to a better acoustic attenuation in the mid frequency range, mainly for low resistivities. As the resistivity of the absorbing material increases, this advantage is gradually reduced. In addition, the presence of a sound-absorbing material in the central chamber of the muffler with empty extended inlet/outlet ducts allows partial retention of the good properties of the dissipative mufflers at higher frequencies, avoiding the TL collapse of purely reactive chambers. The presence of perforated surfaces with reduced porosity produces a detrimental effect on the acoustic performance. Finally, the consideration of larger mufflers leads to a strong effect associated with the propagation of higher-order modes. The attenuation becomes more irregular and a higher number of peaks can be found as the radius is increased. The presence of absorbing material avoids, however, the pass bands commonly found in reactive chambers.

Acknowledgements

UPV's authors wish to thank the financial support of Ministerio de Ciencia y Tecnología by means of project DPI2003-07153-C02-01 and Conselleria d'Empresa, Universitat i Ciència (grant Grupos 04/63). Dr. N.T. Huff and Mr. A. Reinartz, from Owens Corning, are gratefully acknowledged for the support provided with texturized Advantex fiber glass roving.

Appendix A. Direct integration over discrete zones

For the expansion, the integrals associated with Eqs. (19)–(21) are expressed as

$$\sum_{n=0}^{N}(A_n^+ + A_n^-)\int_0^{r_{m,P1}}\psi_{A,n}(r)r^a\,\mathrm{d}r = \sum_{n=0}^{N}(C_n^+ + C_n^-)\int_0^{r_{m,P1}}\psi_{C,n,P}(r)r^a\,\mathrm{d}r, \tag{A.1}$$

$$\begin{aligned}&\sum_{n=0}^{N}B_n^-(\mathrm{e}^{-2\mathrm{j}k_{z,B,n}L_B}+1)\int_{R_1}^{r_{m,P2}}\psi_{B,n}(r)r^a\,\mathrm{d}r - \sum_{n=0}^{N}(C_n^+ + C_n^-)\int_{R_1}^{r_{m,P2}}\psi_{C,n,P}(r)r^a\,\mathrm{d}r\\ &\quad=\frac{c_0\tilde{\zeta}_{p2}}{\omega}\sum_{n=0}^{N}k_{z,B,n}B_n^-(\mathrm{e}^{-2\mathrm{j}k_{z,B,n}L_B}-1)\int_{R_1}^{r_{m,P2}}\psi_{B,n}(r)r^a\,\mathrm{d}r,\end{aligned} \tag{A.2}$$

$$\begin{aligned}&\sum_{n=0}^{N}k_{z,C,n}(C_n^+ - C_n^-)\int_0^{r_{m,U}}\psi_{C,n,U}(r)r^a\,\mathrm{d}r\\ &\quad=\begin{cases}\displaystyle\sum_{n=0}^{N}k_{z,A,n}(A_n^+ - A_n^-)\int_0^{r_{m,U}}\psi_{A,n}(r)r^a\,\mathrm{d}r & \text{for } 0\leqslant r_{m,U}\leqslant R_1,\\ \displaystyle\sum_{n=0}^{N}k_{z,A,n}(A_n^+ - A_n^-)\int_0^{R_1}\psi_{A,n}(r)r^a\,\mathrm{d}r & \\ \quad\displaystyle+\sum_{n=0}^{N}k_{z,B,n}B_n^-(\mathrm{e}^{-2\mathrm{j}k_{z,B,n}L_B}-1)\int_{R_1}^{r_{m,U}}\psi_{B,n}(r)r^a\,\mathrm{d}r & \text{for } R_1\leqslant r_{m,U}\leqslant R_2,\end{cases}\end{aligned} \tag{A.3}$$

where exponent $a = 0$ and 1 denotes the integration over the radius and the area, respectively. Similar integrals are obtained for Eqs. (24)–(26) of the contraction

$$\sum_{n=0}^{N}(E_n^+ + E_n^-)\int_0^{r_{m,P1}}\psi_{E,n}(r)r^a\,\mathrm{d}r = \sum_{n=0}^{N}(C_n^+\mathrm{e}^{-\mathrm{j}k_{z,C,n}L_C} + C_n^-\mathrm{e}^{\mathrm{j}k_{z,C,n}L_C})\int_0^{r_{m,P1}}\psi_{C,n,P}(r)r^a\,\mathrm{d}r, \tag{A.4}$$

$$\begin{aligned}&\sum_{n=0}^{N}(C_n^+\mathrm{e}^{-\mathrm{j}k_{z,C,n}L_C} + C_n^-\mathrm{e}^{\mathrm{j}k_{z,C,n}L_C})\int_{R_1}^{r_{m,P2}}\psi_{C,n,P}(r)r^a\,\mathrm{d}r\\ &\quad-\sum_{n=0}^{N}D_n^+(1+\mathrm{e}^{-2\mathrm{j}k_{z,D,n}L_D})\int_{R_1}^{r_{m,P2}}\psi_{D,n}(r)r^a\,\mathrm{d}r\\ &\quad=\frac{c_0\tilde{\zeta}_{p3}}{\omega}\sum_{n=0}^{N}k_{z,D,n}D_n^+(1-\mathrm{e}^{-2\mathrm{j}k_{z,D,n}L_D})\int_{R_1}^{r_{m,P2}}\psi_{D,n}(r)r^a\,\mathrm{d}r,\end{aligned} \tag{A.5}$$

$$\begin{aligned}&\sum_{n=0}^{N}k_{z,C,n}(C_n^+\mathrm{e}^{-\mathrm{j}k_{z,C,n}L_C} - C_n^-\mathrm{e}^{\mathrm{j}k_{z,C,n}L_C})\int_0^{r_{m,U}}\psi_{C,n,U}(r)r^a\,\mathrm{d}r\\ &\quad=\begin{cases}\displaystyle\sum_{n=0}^{N}k_{z,E,n}(E_n^+ - E_n^-)\int_0^{r_{m,U}}\psi_{E,n}(r)r^a\,\mathrm{d}r & \text{for } 0\leqslant r_{m,U}\leqslant R_1,\\ \displaystyle\sum_{n=0}^{N}k_{z,E,n}(E_n^+ - E_n^-)\int_0^{R_1}\psi_{E,n}(r)r^a\,\mathrm{d}r & \\ \quad\displaystyle+\sum_{n=0}^{N}k_{z,D,n}D_n^+(1-\mathrm{e}^{-2\mathrm{j}k_{z,D,n}L_D})\int_{R_1}^{r_{m,U}}\psi_{D,n}(r)r^a\,\mathrm{d}r & \text{for } R_1\leqslant r_{m,U}\leqslant R_2,\end{cases}\end{aligned} \tag{A.6}$$

with

$$r_{m,P1} = \frac{m}{N+1} R_1, \quad m = 1, ..., N+1, \tag{A.7}$$

$$r_{m,P2} = R_1 + \frac{m}{N+1}(R_2 - R_1), \quad m = 1, ..., N+1, \tag{A.8}$$

$$r_{m,U} = \frac{m}{N+1} R_2, \quad m = 1, ..., N+1. \tag{A.9}$$

The integrals involved in Eqs. (A.1)–(A.6) for $a = 0$ can be easily evaluated by [22]

$$\int_0^{r_0} \psi_0(\lambda r)\,\mathrm{d}r = r_0\psi_0(\lambda r_0) + \tfrac{1}{2}\pi r_0\big(H_0(\lambda r_0)\psi_1(\lambda r_0) - H_1(\lambda r_0)\psi_0(\lambda r_0)\big), \tag{A.10}$$

where

$$\psi_v(\lambda r) = AJ_v(\lambda r) + BY_v(\lambda r), \quad v = 0, 1, \tag{A.11}$$

A and B are constants, and H_0 and H_1 are the zeroth- and first-order Struve functions, whose computation can be carried out by means of the procedures detailed in the work of Zhang and Jin [27].

For $a = 1$, the integrals of Eqs. (A.1)–(A.6) can also be analytically determined in light of [22]

$$\int_0^{r_0} J_0(\lambda r) r\,\mathrm{d}r = \begin{cases} \dfrac{r_0^2}{2}, & \lambda = 0, \\ \dfrac{r_0}{\lambda} J_1(\lambda r_0), & \lambda \neq 0, \end{cases} \tag{A.12}$$

for the zeroth-order Bessel function of the first kind, and

$$\int_0^{r_0} Y_{\upsilon-1}(\lambda r) r^{\upsilon}\,\mathrm{d}r = \frac{r_0^{\upsilon}}{\lambda} Y_{\upsilon}(\lambda r_0) + \frac{2^{\upsilon}}{\pi\lambda^{1+\upsilon}}\Gamma(\upsilon) \tag{A.13}$$

for the zeroth-order Bessel function of the second kind. In Eq. (A.13), $\Gamma(\upsilon)$ is Euler's gamma function, with $\Gamma(1) = 1$.

Appendix B. Comparison of integration approaches

The WI and DI approaches of Section 2.4 and Appendix A, respectively, are analyzed and compared in order to establish their suitability for the acoustic modeling of dissipative mufflers. For this analysis, the TL has been calculated from 10 to 3200 Hz in steps of 10 Hz. The relative error in the TL loss is defined as

$$\mathrm{ETL} = \frac{\sum_{i=1}^{N_f} |\mathrm{TL}_i^{\text{analytical}} - \mathrm{TL}_i^{\mathrm{FEM}}|}{\sum_{i=1}^{N_f} \mathrm{TL}_i^{\mathrm{FEM}}}, \tag{B.1}$$

where the reference value $\mathrm{TL}^{\mathrm{FEM}}$ has been obtained with 8-noded axisymmetric quadrilateral elements and $N_f = 320$. To ensure accurate results from FEM calculations, several computations have been carried out with Sysnoise 5.6, with a refinement ratio of 2.5 [26], until ETL is lower than 0.00025 (geometry 1 without extensions) and 0.0025 (geometry 3 with extensions) between successive refinements. The final mesh, adopted as the reference, has more than 17000 elements and 53000 nodes, with an approximate element size of 0.0015 m, except in the regions close to the expansion and contraction, where the element size has been reduced to 0.0005 m.

Figs. B1(a) and (b) show the error of the DI and WI procedures as a function of the number of modes included in the calculation, for geometries 1 and 3 (see Table 1), respectively, when the presence of fiber with $R = 4896$ rayl/m is considered and no perforated surfaces are included in the analysis. Without extensions, Fig. B1(a), the three procedures exhibit a fast convergence, with WI showing a better performance, followed by DI (with integration over area), with a slightly higher error and some minor oscillations, and finally DI (with integration over radius), which presents a relatively less stable behavior, mainly for a reduced number of

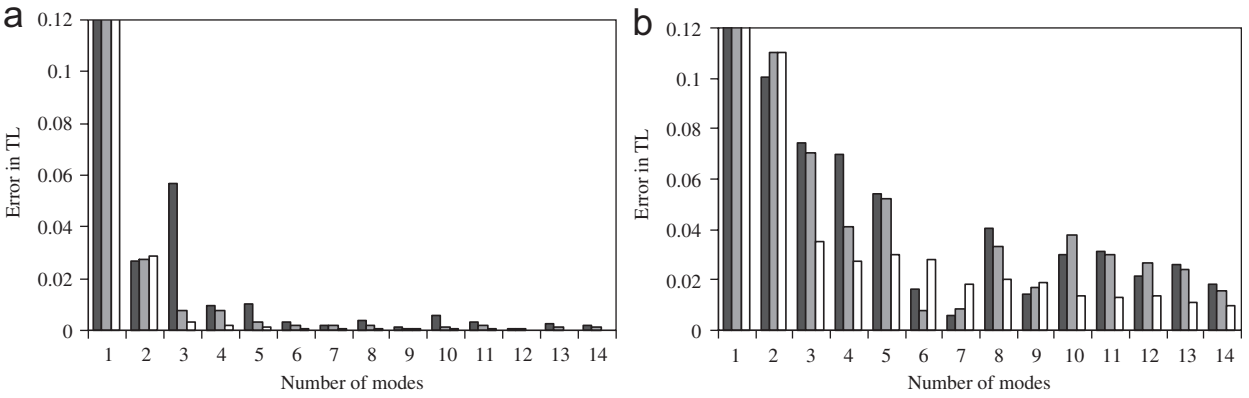

Fig. B1. Error in transmission loss for a muffler with absorbing fiber, $R = 4896$ rayl/m: ■, DI, $a = 0$; ▒, DI, $a = 1$; □, WI. (a) Geometry 1; (b) geometry 3.

modes. The combination of extensions and fiber, depicted in Fig. B1(b), leads to an increase in the deviations for the three procedures, with WI exhibiting a nearly monotonic convergence and a lower error with higher number of modes. The deviations associated with DI for both radius and area integrals are larger along with some oscillations, where a higher number of modes does not necessarily assure a converged solution, at least for the number of modes considered in the figure.

References

[1] M.L. Munjal, *Acoustics of Ducts and Mufflers*, Wiley-Interscience, New York, 1987.
[2] M. Åbom, Derivation of four-pole parameters including higher order mode effects for expansion chamber mufflers with extended inlet and outlet, *Journal of Sound and Vibration* 137 (1990) 403–418.
[3] A. Selamet, Z.L. Ji, Acoustic attenuation performance of circular expansion chambers with extended inlet/outlet, *Journal of Sound and Vibration* 223 (1999) 197–212.
[4] A. Selamet, F.D. Denia, A.J. Besa, Acoustic behavior of circular dual-chamber mufflers, *Journal of Sound and Vibration* 265 (2003) 967–985.
[5] K.S. Peat, K.L. Rathi, A finite element analysis of the convected acoustic wave motion in dissipative silencers, *Journal of Sound and Vibration* 184 (1995) 529–545.
[6] A. Cummings, R.J. Astley, Finite element computation of attenuation in bar-silencers and comparison with measured data, *Journal of Sound and Vibration* 196 (1996) 351–369.
[7] A.F. Seybert, R.A. Seman, M.D. Lattuca, Boundary element prediction of sound propagation in ducts containing bulk absorbing materials, *Journal of Vibration and Acoustics* 120 (1998) 976–981.
[8] T.W. Wu, C.Y.R. Cheng, Z. Tao, Boundary element analysis of packed silencers with protective cloth and embedded thin surfaces, *Journal of Sound and Vibration* 261 (2003) 1–15.
[9] C.N. Wang, Numerical decoupling analysis of a resonator with absorbent material, *Applied Acoustics* 58 (1999) 109–122.
[10] K.S. Peat, A transfer matrix for an absorption silencer element, *Journal of Sound and Vibration* 146 (1991) 353–360.
[11] R. Kirby, Simplified techniques for predicting the transmission loss of a circular dissipative silencer, *Journal of Sound and Vibration* 243 (2001) 403–426.
[12] A. Cummings, I.J. Chang, Sound attenuation of a finite length dissipative flow duct silencer with internal mean flow in the absorbent, *Journal of Sound and Vibration* 127 (1988) 1–17.
[13] M.B. Xu, A. Selamet, I.J. Lee, N.T. Huff, Sound attenuation in dissipative expansion chambers, *Journal of Sound and Vibration* 272 (2004) 1125–1133.
[14] A. Selamet, M.B. Xu, I.J. Lee, N.T. Huff, Analytical approach for sound attenuation in perforated dissipative silencers, *Journal of the Acoustical Society of America* 115 (2004) 2091–2099.
[15] R. Glav, The transfer matrix for a dissipative silencer of arbitrary cross-section, *Journal of Sound and Vibration* 236 (2000) 575–594.
[16] R. Kirby, Transmission loss predictions for dissipative silencers of arbitrary cross section in the presence of mean flow, *Journal of the Acoustical Society of America* 114 (2003) 200–209.
[17] I.J. Lee, Acoustic characteristics of perforated dissipative and hybrid silencers, PhD Thesis, Ohio State University, 2005.
[18] A. Selamet, I.J. Lee, N.T. Huff, Acoustic attenuation of hybrid silencers, *Journal of Sound and Vibration* 262 (2003) 509–527.
[19] A. Selamet, M. Xu, I.J. Lee, N.T. Huff, Analytical approach for sound attenuation in perforated dissipative silencers with inlet/outlet extensions, *Journal of the Acoustical Society of America* 117 (2005) 2078–2089.

[20] F.D. Denia, A. Selamet, F.J. Fuenmayor, R. Kirby, Sound attenuation in partially-filled perforated dissipative mufflers with extended inlet/outlet, *Proceedings of the 12th International Congress on Sound and Vibration*, Lisbon, Portugal, 2005.
[21] F.P. Mechel, *Formulas of Acoustics*, Springer, Berlin, 2002.
[22] M. Abramowitz, I.A. Stegun, *Handbook of Mathematical Functions*, Dover Publications, New York, 1972.
[23] J.W. Sullivan, M.J. Crocker, Analysis of concentric-tube resonators having unpartitioned cavities, *Journal of the Acoustical Society of America* 64 (1978) 207–215.
[24] J.L. Bento, Acoustic characteristics of perforate liners in expansion chambers, PhD Thesis, University of Southampton, 1983.
[25] R. Kirby, A. Cummings, The impedance of perforated plates subjected to grazing gas flow and backed by porous media, *Journal of Sound and Vibration* 217 (1998) 619–636.
[26] F.J. Fuenmayor, F.D. Denia, J. Albelda, E. Giner, H-adaptive refinement strategy for acoustic problems with a set of natural frequencies, *Journal of Sound and Vibration* 255 (2002) 457–479.
[27] S. Zhang, J. Jin, *Computation of Special Functions*, Wiley-Interscience, New York, 1996.